Chinese Journal of
POLYMER SCIENCE

RESEARCH ARTICLE

https://doi.org/10.1007/s10118-026-3802-7
Chinese J. Polym. Sci.

Translocation of a Long Passive Polymer Chain through a Small Pore Pulled by an Active Polymer Chain

Yan-Li Zhou, Xiao Yang, Bin Zhao, and Chao Wang*

Department of Physics, Taizhou University, Taizhou 318000, China

Abstract The translocation of a long passive polymer chain (polymer P) through a small pore pulled by an active polymer chain (polymer A) was studied *via* simulation. The results indicate that the translocation dynamics of polymer P is strongly correlated with the conformation state of polymer A during the translocation process, depending on the active force f_a and the rigidity k_b of polymer A. For the case k_b is very small (including k_b=0), polymer A is nearly a random coil at small f_a, and forms a stable spiral at large f_a. When f_a is small, it is very difficult for polymer A to pull polymer P through the pore, and the translocation time (τ) is large. When f_a is large, τ is small, and the translocation dynamics is determined by a winch-driven mechanism, where the spiral of polymer A rotates synchronously, pulling polymer P through the pore and winding it sequentially around itself. When k_b is large, polymer A adopts a rod configuration, and the translocation of polymer P is controlled by the translation of the polymer A rod.

Keywords Active polymer; Translocation; Dynamics; Simulation

Citation: Zhou, Y. L.; Yang, X.; Zhao, B.; Wang, C. Translocation of a long passive polymer chain through a small pore pulled by an active polymer chain. *Chinese J. Polym. Sci.* https://doi.org/10.1007/s10118-026-3802-7

INTRODUCTION

The translocation of polymers through small pores is universal in many biological processes, such as gene expression, DNA and RNA translocation through the nuclear pores, protein moving across membrane channels, transfer of genes between bacteria, *etc*.,[1–8] and is also related to many technological applications, such as drug delivery, genome mapping, DNA sequencing and separation, *etc*.[9–16] Consequently, it has been a hot topic and attracted lots of attention in the last two decades.

In real systems, the nanopores are much smaller than the polymer, making spontaneous translocation difficult. Therefore, an external force is often required to drive the transport of the polymer through the pores. Most experiments considered an external electric field as the driving force for DNA translocation.[17–19] However, a variety of other driving mechanisms have been explored in previous studies, including fluid flow,[20–23] particle binding,[24–26] spatial confinement,[27–29] end-pulling force,[30–39] *etc*.

In studies of polymer translocation, the dependence of the translocation time (τ) on the polymer chain length (N) and driving force (f) has been extensively studied. It was found that τ as a function of N and f can be expressed as $\tau \propto N^{\alpha} f^{-\delta}$. For the case in which the driving force is confined inside the pore, many studies have predicted that α is between 2ν and $1+\nu$ (ν is the Flory exponent), depending on the strength of the driving force,[40–44] and δ~1 for small f and δ~0.8 for large f.[44,45] When the driving force is exerted at the head of the polymer chain, it was found that α=2 and δ=–2+1/ν for moderate f, and α=2 and δ=–1 for large f.[30–33] Recently, Hu *et al*. studied the translocation of the polymer chain driven by an active Brownian particle (ABP), and found that the effect of the ABP on the translocation differs significantly from the driving force inside the pore or at the head for traditional polymer translocations. Specifically, δ=–1 for large f_s. Moreover, it was found that α~2.5 for small f or large N and α~1.4 for large f and small N.[39]

In recent years, the conformation and dynamics of active polymers (including polar and nonpolar polymers) have been extensively studied. In two-dimensional (2D) free space, the active polymers can spontaneously form stable spirals at a strong active force and low rigidity, and exhibit rich movement. In particular, the active polymer barely moves in spiral states and exhibits net displacements in a railway motion manner in non-spiral states, and an optimal active force exists that maximizes the diffusion coefficient.[46–50] In three-dimensional (3D) free space, active polymers undergo a coil-globule or inflation-collapse transition with increasing the active force, and the diffusion coefficient of the polymer is independent of the polymer length for long polymers or large active forces.[51,52]

Under spatially restricted conditions, the active polymers exhibit complex properties. When the head of the polymer is fixed, it exhibits a spiral form with rotational motion or a wave form with flapping motion.[53–56] While when the end of the polymer is fixed, it undergoes continuous self-knotting. Once

* Corresponding author, E-mail: chaowang0606@126.com
Received May 18, 2026; Accepted July 3, 2026; Published online September 20, 2026

a knot is formed, it migrates gradually to the anchoring point. Moreover, when the end of the active polymer is grafted on a passive polymer, it can function as a self-propelling soft needle to either transfer its own knots or braid knots directly on the passive polymer.[57,58] In the presence of obstacle(s), active polymers exhibit diverse conformations and motion types. In particular, in an environment with multiple obstacles, active polymers with different activity and rigidity exhibit different diffusion dynamics, which are useful for the separation of active polymers.[59–63] For active polymer confined in a circular cavity, it forms a stable compact spiral at a large active force. It was found that the formation of the stable compact spiral is a two-step relaxation process in which the polymer first forms a metastable swelling quasi-spiral and then transforms into the stable compact spiral near the wall of the cavity. In particular, when the circumference of the circle is nearly equivalent to the polymer length, it takes a long time for the polymer to form the compact spiral.[64]

Recently, it has been found that active polymers can spontaneously translocate through narrow pores. When the pore is short, the polymer undergoes railway motion during the translocation process, and the translocation time has a simple power-law dependence on the polymer length and the active force, with α=1 and δ=–1.[65] While when the pore is long, the translocation time shows a non-monotonic change with increasing pore width, owing to the crucial interplay of activity and spatial confinement.[66] For active polymers confined in a transverse asymmetric channel, the transport direction of the polymer can be rectified and even show current reversals.[67] For an active polymer translocating into a small circular cavity, it was found that the translocation dynamics of the active polymer shows a strong correlation with the polymer conformation inside the cavity. When the polymer rigidity k_b is small, the polymer is a nearly random coil in the cavity, and the translocation time is long. While when k_b is moderate or large, the polymer inside the cavity forms a spiral configuration and the entire polymer moves synchronously, which is helpful for translocation.[68,69]

In addition to its complex motion manners of itself, an active polymer can drive passive objects. Several groups have attached a passive load to an active filament and found versatile dynamic motion modes, including elongated, rotating, beating, and beat-and-circle motions.[70,71] Such "active-passive" composite models may be related to several biological systems. For example, during gene expression, motor proteins actively pull RNA to the vicinity of the nuclear pore complex. Similarly, during bacterial conjugation, motor proteins pull the donor DNA strand into the recipient cell. Inspired by this, we here construct an "active-passive" diblock copolymer, and study the translocation of the passive polymer (the passive block) through a small pore pulled by the active polymer (the active block). Our model represents a simplified "active-passive" composite system. Different from Refs. [70] and [71], the passive part (the load) in our model is a polymer chain rather than a solid particle.

Our results indicate that the translocation dynamics is strongly correlated with the configuration of the active polymer. In particular, when the active force is large, the flexible active polymer forms a stable spiral during translocation. Under the driving of the active force, the polymer spiral functions as a soft winch: it synchronously rotates and winds the passive polymer chain, pulling it through the pore. This winch-driven translocation mechanism leads to a distinct scaling law and a final composite spiral structure, which has not been previously reported. Thus, our results provide new insights into the driven translocation of polymer chains, where the active polymer acts as a self-organizing, torque-generating engine.

SIMULATION MODELS AND METHODS

The simulation was performed in a 2D space. Fig. 1 shows a sketch of the model system. The entire space was divided into two parts, the *cis* and *trans* sides, by an infinite wall at x=0. The wall is a single stationary layer of closely packed particles with diameter σ, yielding an effective wall thickness of σ. In the middle of the wall, there is a pore with width w_p and length (*i.e.*, the wall thickness) σ. The polymer chain is initially generated on the *cis* side, and it can only translocate from the *cis* side to the *trans* side through the pore.

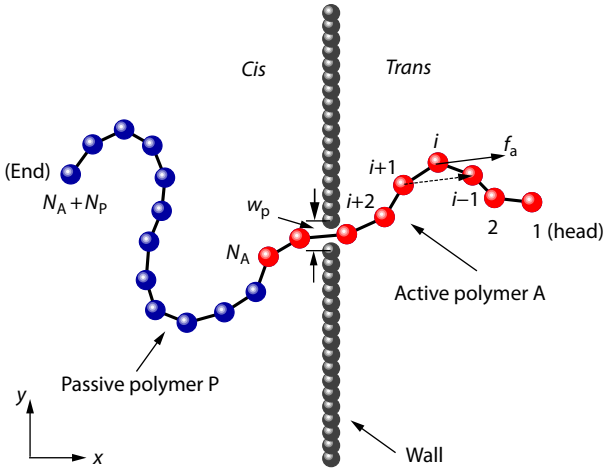

Fig. 1 A sketch of the simulation model system. The *cis* side and the *trans* side are connected by a narrow pore with width w_p in the middle of an infinite flat wall. The polymer chain is composed of identical beads connected sequentially, and it contains two sub-chains, an active polymer chain (polymer A) with length N_A and a passive polymer chain (polymer P) with length N_P. The i^{th} monomer ($1<i<N_A$) of polymer A experiences a tangential active force f_a along the vector $\boldsymbol{r}_{i-1,i+1}$ between the positions of the monomers i–1 and i+1. Polymer P can translocate from the *cis* side to the *trans* side through the pore under the drive of polymer A.

In our simulation, the polymer chain was mimicked by a coarse-grained bead-spring chain model. The polymer chain is composed of N_A+N_P identical beads (or monomers) connected sequentially by bonds, and it contains two sub-chains: an active polymer chain (polymer A) with length N_A and a passive polymer chain (polymer P) with length N_P.

The interaction between any two monomers is described by the purely repulsive Weeks-Chandler-Andersen (WCA) potential (Eq. 1):

$$U_{WCA}(r)=\begin{cases}4\varepsilon_0\left[\left(\frac{\sigma}{r}\right)^{12}-\left(\frac{\sigma}{r}\right)^{6}\right]+\varepsilon_0 & \text{for } r\le r_{cutoff}\\ 0 & \text{for } r>r_{cutoff}\end{cases} \quad (1)$$

where r is the distance between the two monomers, ε_0 is the interaction strength, σ is the diameter of the monomers, and $r_{cutoff} = 2^{1/6}\sigma$ is the cut-off distance. The bond interaction between any two bonded monomers can be described simply by the elastic potential (Eq. 2):

$$U_{bond}(b) = k(b - b_0)^2 \quad (2)$$

where k is the spring constant, and b and b_0 represent the bond length and equilibrium bond length, respectively.

In our model, polymer P was flexible, and polymer A was semi-flexible. The bending energy between any two adjacent bonds of polymer A is described by (Eq. 3):

$$U_{bend} = k_b\theta^2 \quad (3)$$

where θ is the angle between two neighboring bond vectors, k_b is the bending rigidity. The rigidity of polymer A was determined by k_b. Polymer A is completely flexible at k_b=0. However, polymer A becomes more and more rigid with increasing k_b, and tends to be rod-like at infinite k_b. Here, we treat the bending rigidity k_b as an independent parameter. This allowed us to systematically study the transition of polymer A from a spiral to a rod under the same activity, which is crucial for understanding how the conformation of polymer A influences the translocation of polymer P.

To model the activity of polymer A, we assume that the i^{th} monomer ($1<i<N_A$) experiences a self-propelled tangential force (Eq. 4).[47,57–59,64,65]

$$\boldsymbol{F}_a^{(i)} = f_a\frac{\boldsymbol{r}_{i-1,i+1}}{|\boldsymbol{r}_{i-1,i+1}|} \quad (4)$$

Here, $f_a \geq 0$ represents the strength of the active force, and $\boldsymbol{r}_{i-1,i+1} = \boldsymbol{r}_{i-1} - \boldsymbol{r}_{i+1}$ is the vector between the positions of monomers i–1 and i+1. The activity of polymer A is dependent on f_a, that is, polymer A becomes more and more active with increasing f_a. For i=1 and N_A, we assume that $\boldsymbol{F}_a^{(i)} = 0$.

The interaction between any monomer of the polymer and the particle of the wall is also described by the WCA potential (Eq. 1), where r represents the distance between the polymer monomer and the wall particle.

The motion of each monomer is described by the Langevin equation (Eq. 5):

$$m\frac{d\boldsymbol{v}}{dt} = -\nabla(U_{WCA} + U_{bond} + U_{bend}) + \boldsymbol{F}_a - \eta\boldsymbol{v} + \boldsymbol{F}^T \quad (5)$$

Here m is the mass of the monomer, η is the friction coefficient, and $\boldsymbol{F}^T$ is the random force with $\langle\boldsymbol{F}^T(t)\rangle = 0$ and $\langle\boldsymbol{F}^T(t)\cdot\boldsymbol{F}^T(t')\rangle = 4\eta k_B T\delta(t-t')$, where k_B and T represent the Boltzmann constant and the temperature, respectively. For the numerical integration of Eq. (5), the velocity Verlet algorithm was adopted with a time step Δt=0.005.

At the beginning of the simulation, we generated the polymer chain in the *cis* side, with the head monomer (i=1) being fixed in the middle of the pore. We first let the polymer chain undergo a long equilibrating time (=10^6) of Brownian motion with f_a=0, and then turn on the active force and let the polymer chain undergo a long steadying time (>10^6) to reach the final steady-state, under the constraint that the head monomer is fixed. We finally released the head monomer and monitor the movement of the polymer chain.

Since the head monomer (the first monomer of polymer A) is initially in the pore, polymer A can translocate through the pore driven by the tangential active force and then pull polymer P into the *trans* side. During the translocation process, the head of polymer A may go back to the *cis* side under random thermal fluctuations. In this case, we stopped the simulation and began a new run until a successful translocation of polymer P occured eventually. In this work, we define the translocation time τ of polymer P as the conditional time from the last entry of the N_A^{th} monomer of polymer A into the *trans* side to the first entry of the last monomer of polymer P into the *trans* side for successful translocation events only. All the statistical results in our work were averaged over 200–2000 independent successful translocation runs.

In this study, σ, m, and k_BT are chosen as the units of length, mass, and energy, respectively. Therefore, the time scale and force scale are defined by $t_{LJ} = (m\sigma^2/k_BT)^{1/2}$ and $f_0 = k_BT/\sigma$, respectively. In the simulation, we set ε_0=1, k=1000, b_0=1, and set the friction coefficient η=10 to ensure the overdamped motion of the monomers. Moreover, to ensure the monomers move across one by one, we chose a narrow pore with width w_p=2.4. We mainly studied the influence of f_a, k_b, N_A and N_P on the translocation dynamics of polymer P through the narrow pore.

SIMULATION RESULTS AND DISCUSSION

Completely Flexible Polymer A (k_b=0)

First, we studied the translocation of polymer P pulled by completely flexible polymer A with k_b=0. Fig. 2 shows the typical distribution of translocation times for small f_a (=0.4) and large f_a (=4), respectively, where N_A=20 and N_P=100. For f_a=0.4, the distribution is broad and asymmetric, and has a long tail, which is similar to that for the free translocation case.[33] While for large f_a=4, the distribution is narrow and nearly symmetric, which is similar to that for the end-pulling translocation case.[33] We can also see that, for both small and large f_as, the average translocation time is very close to the most probable translocation time. Therefore, the average translocation time is well defined to describe the dynamics of the translocation of polymer P.

Fig. 3 shows the dependence of the translocation time τ on the active force f_a for different length N_A of polymer A, where the length of polymer P is N_P=100. We can see that τ is very large at small f_a and N_A, indicating that it is difficult for polymer P to translocate through the pore when polymer A is short and the activity is weak. With f_a or N_A increasing, τ decreases monotonically. In our model, the translocation of polymer P through the pore is pulled by polymer A. Because the active force acts on each monomer of polymer A (except for the 1st and N_A^{th} monomers), the effective driving force exerting on polymer P increases with f_a or N_A increasing, leading to the decrease of τ with f_a or N_A, as shown in Fig. 3. Interestingly, for small N_A (=10, 15, and 20), there is an obvious transition on the curve of τ with f_a at moderate f_a, indicating that the translocation model at large f_a may be different from that at small f_a. With N_A increasing, the transition becomes smoothed gradually. In particular, in the large f_a region, the dependence of τ on f_a for different N_A can be described by a simple scaling relation $\tau \propto f_a^{-1}$.

We have studied the dependence of the translocation time τ on the length N_P of polymer P at small f_a and large f_a. As ex-

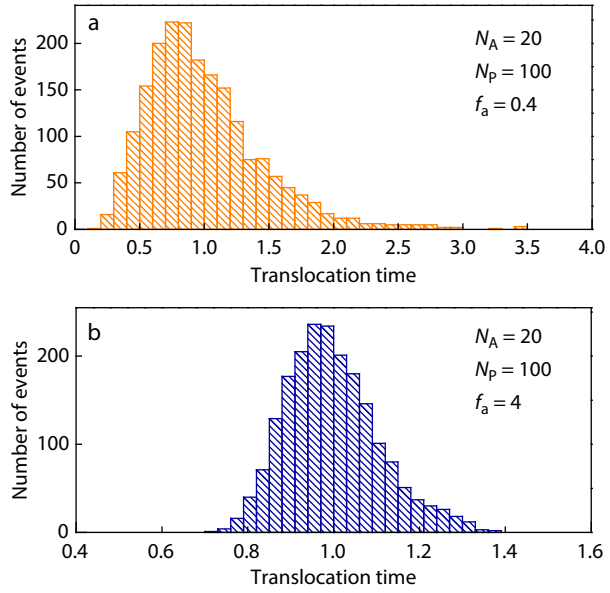

Fig. 2 Distribution of translocation times for (a) f_a=0.4 and (b) f_a=4, where N_A=20 and N_P=100. The translocation times were normalized by their average values.

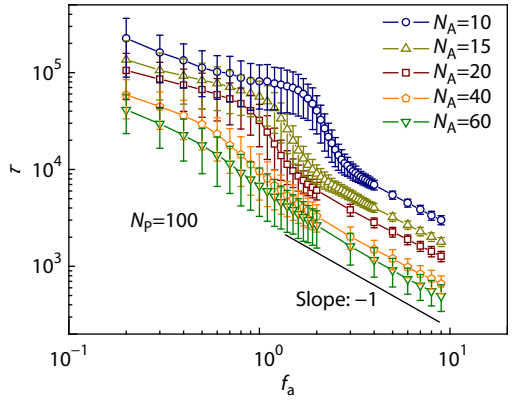

Fig. 3 Dependence of the translocation time τ on the active force f_a for different lengths N_A of polymer A, where the length of polymer P was N_P=100. Error bars correspond to standard deviations.

amples, Fig. 4 shows the results for a small f_a=0.4 (Fig. 4a) and a large f_a=4 (Fig. 4b). For any given N_A and f_a, τ increases monotonously with N_P increasing, indicating that a longer polymer P always spends a longer time completing the translocation process. When f_a is small, the increase of τ with N_P is remarkable, indicating that it is very difficult for polymer A with weak activity to pull long polymer P through the pore completely. In particular, in the large N_P region, the dependence of τ on N_P can be described by the power law $\tau \propto N_P^{3.1}$, as shown in the inset of Fig. 4(a). Comparing with the result for small f_a, the increase of τ with N_P for large f_a is relatively slow, meaning that polymer A with strong activity can easily drive polymer P through the pore. Interestingly, we found that τ for different N_A at large f_a nearly collapsed on a main curve for τ/N_A versus N_P/N_A, as shown in the inset of Fig. 4(b).

To understand the dependence of τ on f_a, we have studied the details of the translocation process. For examples, Fig. 5

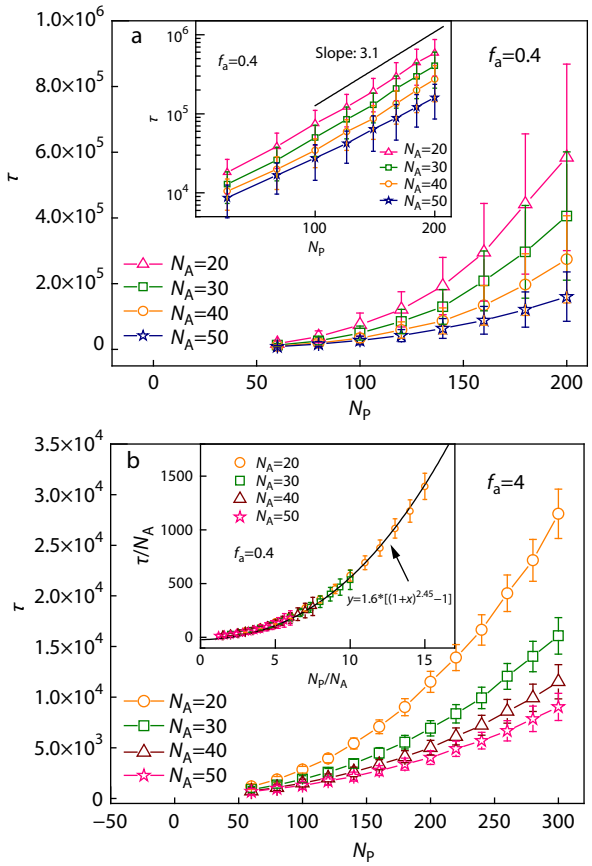

Fig. 4 Dependence of the translocation time τ on the length N_P of polymer P for (a) f_a=0.4 and (b) f_a=4. The inset of (a) presents the log-log plots of τ with N_P for f_a=0.4. The inset of (b) shows the dependence of τ/N_A on N_P/N_A for f_a=4, where the solid line represents the fitting line. Error bars correspond to standard deviations.

shows a series of snapshots of polymer A and polymer P for f_a=0.4 (Fig. 5a) and 4 (Fig. 5b), respectively, at different times of a translocation sample, where N_A=20 and N_P=100. We can see that, during the translocation process, polymer A shows different configuration states depending on the strength of the active force. For f_a=0.4 (small f_a), it adopts a random coil configuration. While for f_a=4 (large f_a), it forms a spiral configuration. These results are similar to those for active polymers in 2D free space.[47] When f_a is small, the polymer behaves like a passive polymer and is in the coil configuration state. When f_a is large, the head part of the active polymer can be forced to bend by colliding with a subsequent part of the polymer, and then the entire polymer winds inward by further driven by the tangential active force, leading to the emergence of the stable spiral configuration state.

To further show the correlation between the translocation dynamics and the configuration of polymer A, we have calculated the spiral parameter C_S of polymer A at the end of the translocation process, which is defined as Eq. (6).

$$C_S = \frac{1}{N_A - 2}\left|\sum_{i=1}^{N_A-2} \frac{\boldsymbol{r}_{i,i+1} \times \boldsymbol{r}_{i+1,i+2}}{|\boldsymbol{r}_{i,i+1} \times \boldsymbol{r}_{i+1,i+2}|}\right| \quad (6)$$

where $\boldsymbol{r}_{i,i+1}$ represents the bond vector between the i^{th} and

https://doi.org/10.1007/s10118-026-3802-7

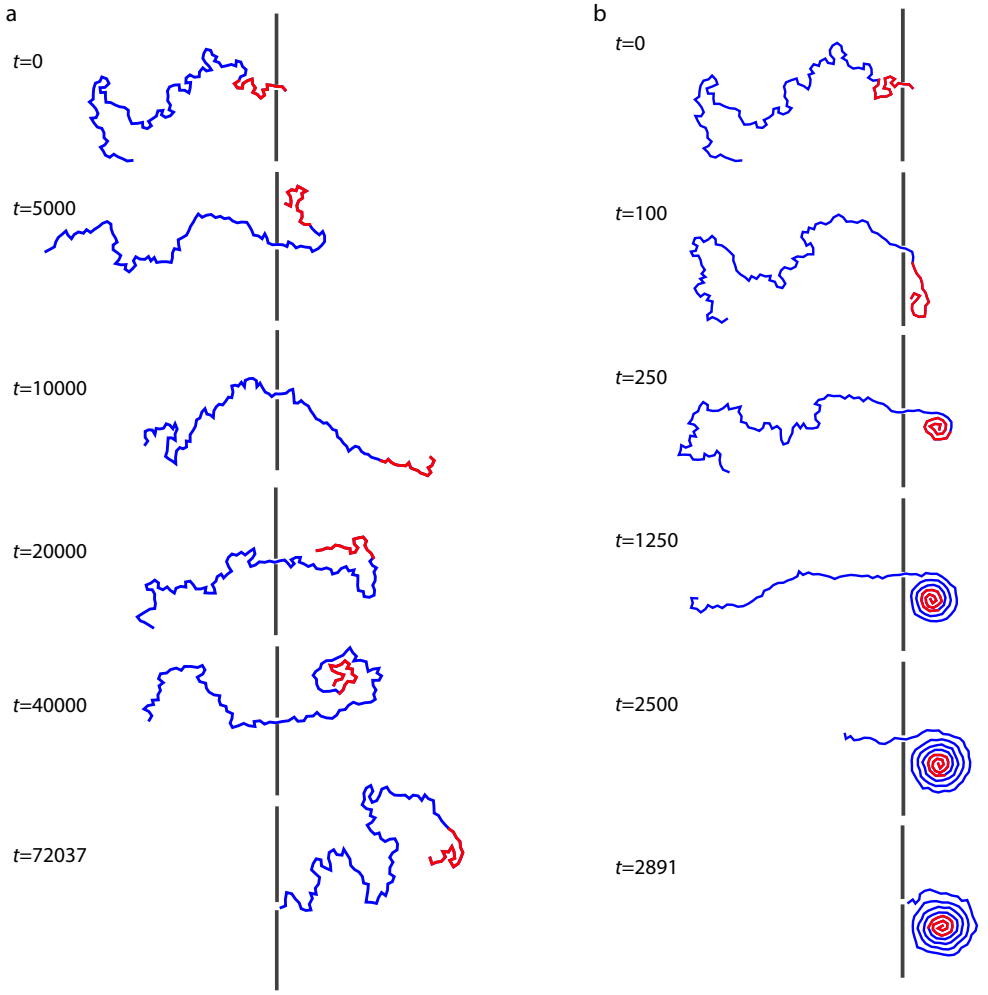

Fig. 5 A series of snapshots of polymer A and polymer P for (a) f_a=0.4 and (b) f_a=4 at different times for a translocation sample, where N_A=20 and N_P=100.

$(i+1)^{th}$ monomers, and $\boldsymbol{r}_{i+1,i+2}$ represents the bond vector between the $(i+1)^{th}$ and $(i+2)^{th}$ monomers. $C_S \to 0$ for the random coil state, and $C_S \to 1$ for the stable spiral state. As an example, Fig. 6 shows the dependence of C_S on f_a, where N_A=20 and N_P=100. Moreover, the dependence of τ on f_a for the same parameter set is also shown for comparison purpose. We can see that C_S is very small at small f_a region, meaning that polymer A is nearly in the coil state and tends to be 1 at large f_a region, indicating that polymer A is in the spiral state. Specially, with f_a increasing, C_S increases quickly near f_a~1.2, where τ shows a rapid decrease, as shown in Fig. 6. Our results indicated that the translocation dynamics of polymer P is related to the configuration of polymer A.

The difference in the configuration of polymer A at small f_a and large f_a may lead to different translocation dynamics of polymer P. When f_a is small, polymer A is in the coil state and undergoes nearly random diffusion during the translocation process, which will produce a very small pulling force on polymer P. Therefore, the translocation of polymer P can be approximated as a random diffusion process, resulting in a very large translocation time. Based on the free energy landscape of the polymer during the translocation process, Sung and Park obtained the translocation time by calculating the

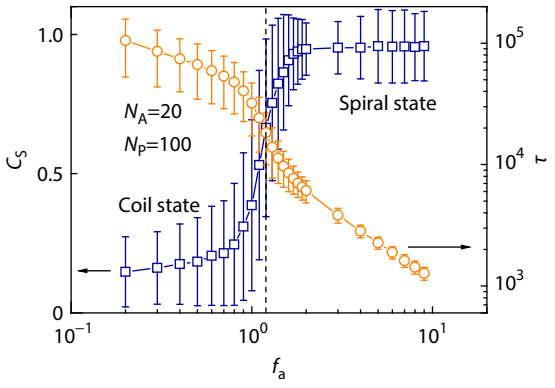

Fig. 6 Dependence of the spiral parameter C_S and the translocation time τ on f_a, where N_A=20 and N_P=100. Error bars correspond to standard deviations.

Fokker-Planck equation and found that the dependence of the translocation time on the polymer length can be described by a power law, $\tau \propto N^3$, when the driving force is zero or very small,[72] which is in good agreement with our simulation results, as shown in the inset of Fig. 4(a).

When f_a is large, polymer A is in spiral state, and the tan-

https://doi.org/10.1007/s10118-026-3802-7

gential active force will produce an effective force torque to drive polymer A rotating around its mass center. In this case, polymer A acts as a rotating winch, pulling polymer P through the pore quickly. Meanwhile, the part of polymer P that has entered into the *trans* side will sequentially wrap around the exterior of polymer A and follow its rotation. At the end of the translocation, there will be a large stable spiral with polymer A constituting the inner core and polymer P surrounding it. This is a new driven mechanism, and we call it the winch-driven mechanism. Qualitatively, the effective force torque acting on polymer A increases with the increase in the active force and the length of polymer A, leading to the decrease of the translocation time with f_a and N_A increasing, as shown in Fig. 3.

To understand the rotation of the polymer A spiral, we have calculated the angular $\Delta\theta$ between $\boldsymbol{R}_A(t)$ and $\boldsymbol{R}_A(0)$, where $\boldsymbol{R}_A(t)$ and $\boldsymbol{R}_A(0)$ represent the end-to-end vector of polymer A at times t and 0, respectively. The typical result of the time evolution of $\Delta\theta$ during one successful translocation process is shown in Fig. 7. At the early stage of the translocation process, $\Delta\theta$ is small and exhibits strong oscillations, because the spiral structure of polymer A has not yet been formed. After the formation of the spiral of polymer A, the spiral undergoes directional rotation under the drive of the active force, leading to the monotonous increase in $\Delta\theta$ and periodic variation in $\sin(\Delta\theta)$, as shown in Fig. 7. During the translocation process, as more passive monomers enter the *trans* side, the spiral expands and the rotational friction increases, leading to a gradual slow down in the rotation of the spiral. This manifests as a slower increase in $\Delta\theta$ and a growing period of $\sin(\Delta\theta)$, as shown in Fig. 7. That is, the angular velocity of the spiral is not constant, but keeps decreasing gradually.

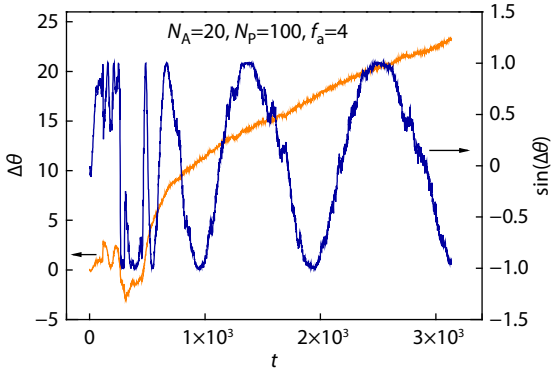

Fig. 7 Evolution of $\Delta\theta$ and $\sin(\Delta\theta)$ during a successful translocation process, where N_A=20, N_P=100, and f_a=4.

The dependence of τ on f_a, N_A, and N_P at large f_a region can be understood quantitatively using the following dynamical model. When f_a is large, the translocation of polymer P is controlled by the winch-driven mechanism, and monomers in the *trans* side form a rotating spiral. Assuming that the polymer spiral containing n monomers can be seen as a uniform disk with radius R_s and mass M, the average radius of the monomers with respect to the disk center (or the mass center (MC) of the polymer spiral) can be expressed as Eq. (7).

$$\bar{r} = \frac{\sum_{i=1}^{n} r_i}{n} = \int_0^{R_s} \frac{r\sigma_s 2\pi r dr}{M} = \frac{2}{3}R_s \tag{7}$$

where r_i represents the distance between the i^{th} monomer and the MC, and the surface density $\sigma_s = M/2\pi R_s^2$. The square radius of gyration of the spiral can also be described by Eq. (8).

$$R_{gs}^2 = \overline{r^2} = \frac{\sum_{i=1}^{N} r_i^2}{n} = \int_0^{R_s} \frac{r^2\sigma_s 2\pi r dr}{M} = \frac{1}{2}R_s^2 \tag{8}$$

Similarly, the average radius of polymer A monomers with respect to the disk center can be expressed as Eq. (9).

$$\overline{r_a} = \frac{\sum_{i=1}^{N_A} r_i}{N_A} = \int_0^{R_{sA}} \frac{r\sigma_s 2\pi r dr}{M_A} = \frac{2}{3}R_{sA} \tag{9}$$

where R_{sA} and M_A represent the radius and the mass of the polymer A spiral, respectively.

Under the driving of the tangential active force, the polymer spiral rotates around its MC. The active force torque with respect to the MC is

$$M_a = f_a \sum_{i=2}^{N_A-1} r_i \approx N_A f_a \overline{r_a} = \frac{2}{3}N_A f_a R_{sA} \tag{10}$$

and the friction force torque with respect to the MC is

$$M_f = \sum_{i=1}^{n} \eta\omega r_i^2 = n\eta\omega\overline{r^2} = \frac{1}{2}n\eta\omega R_s^2 = \frac{1}{2}n\eta v R_s \tag{11}$$

where ω is the angular velocity of the spiral, and v is the linear velocity of the outermost layer of the spiral.

In the overdamped limit, the active force torque is balanced by the friction force torque, *i.e.*, $M_a = M_f$, so we can obtain from Eqs. (10) and (11) that

$$v \propto \frac{f_a N_A R_{sA}}{\eta n R_s} \tag{12}$$

It has been proven that R_{gs} of a polymer spiral as a function of the polymer length N can be described by a power-law relation $R_{gs} \propto N^{0.43}$.[59,64] So, we have

$$R_s \propto n^{0.43} \text{ and } R_{sA} \propto N_A^{0.43} \tag{13}$$

Then, we can obtain from Eqs. (12) and (13) that,

$$v \propto \frac{f_a N_A^{1.43}}{\eta n^{1.43}} \tag{14}$$

In our model, v can also be considered as the translocation velocity of polymer P, *i.e.*, $v \propto \frac{dn}{dt}$, and then we can obtain from Eq. (14) that

$$\frac{dn}{dt} \propto \frac{f_a N_A^{1.43}}{\eta n^{1.43}} \tag{15}$$

and

$$\int_0^{\tau} dt \propto \int_{N_A}^{N_A+N_B} \frac{\eta n^{1.43}}{f_a N_A^{1.43}} dn \tag{16}$$

We can calculate the translocation time τ from Eq. (16),

$$\tau \sim \frac{\eta}{f_a N_A^{1.43}} \left[(N_A + N_P)^{2.43} - N_A^{2.43} \right] \tag{17}$$

or

$$\frac{\tau}{N_A} \sim \frac{\eta}{f_a} \left[\left(1 + \frac{N_P}{N_A} \right)^{2.43} - 1 \right] \tag{18}$$

This result is in good agreement with the simulation results shown in Figs. 3 and 4(b). Specially, when $N_P >> N_A$, we

obtain from Eq. (18) that

$$\tau \propto \frac{N_P^{2.43}}{f_a N_A^{1.43}} \tag{19}$$

The extended nature of polymer A is crucial for the winch-driven mechanism. If we replace polymer A with a single active monomer (*i.e.*, N_A=3) pulling polymer P, the system reduces to the well-studied end-pulling translocation, and the scaling law between τ and N_P will be $\tau \propto N_P^2$ (result not shown). Moreover, a single active monomer cannot generate the torque required for the winch action, nor can it wind the passive chain around itself.

Semiflexible Polymer A (k_b>0)

We have studied the influence of the rigidity (k_b) of polymer A on the translocation dynamics when f_a is large. Qualitatively, it is more and more difficult for polymer A to form a stable spiral with k_b increasing. Fig. 8 shows the typical results for the dependence of the radius of gyration (R_{gA}) of polymer A at the end of the translocation process on the rigidity k_b, where f_a=4, N_A=20, and N_P=100. When k_b is very small, polymer A is in the stable spiral state, resulting that R_{gA} is small. While when k_b is large, R_{gA} maintains a large value (about 5.8, which is nearly the same as that of a rod-like polymer with N_A=20), indicating that polymer A forms a rod-like configuration. Near a specific k_b^* (about 4), there is an obvious transition. We would note that the transition becomes smoothed gradually with N_A increasing (results not shown). Interestingly, with k_b increasing, the translocation time τ also shows an obvious transition near k_b^* from a large value to a small value (as shown in Fig. 8), which indicates once more that the translocation dynamics of polymer P is strongly correlated with the configuration of polymer A. Moreover, we find that the value of τ at large k_b region is much smaller than that of τ at small k_b region, meaning that a rod-like polymer A can pull polymer P through the pore more quickly than a spiral polymer A.

To further study the translocation dynamics of polymer P pulling by a rod-like polymer A, we have carried out simulations at large k_b and f_a. As an example, Fig. 9 shows the dependence of the translocation time τ on the length N_P of polymer P for different N_A, where k_b=50 and f_a=4. Similar to

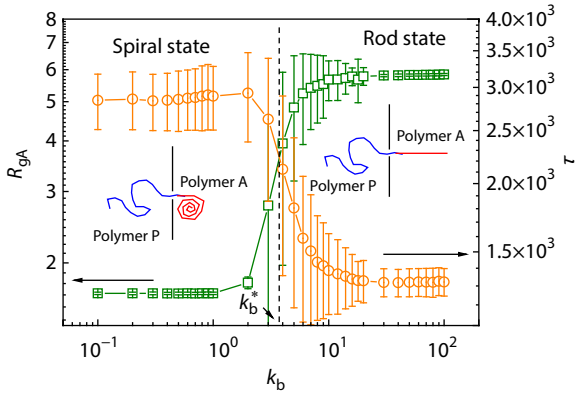

Fig. 8 Dependence of R_{gA} of polymer A at the end of the translocation process and the translocation time τ on the rigidity k_b, where f_a=4, N_A=20, and N_P=100. Error bars correspond to standard deviations.

the results for k_b=0, τ increases monotonously with N_P increasing or N_A decreasing, and τ for different N_A nearly collapse on a main curve for τ/N_A versus N_P/N_A, as shown in Fig. 9.

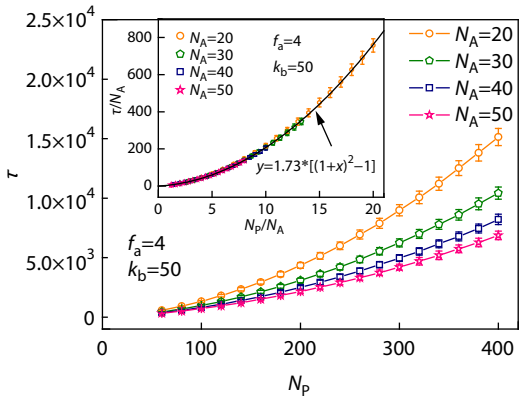

Fig. 9 The dependence of the translocation time τ on the length N_P of polymer P for different N_A, where k_b=50 and f_a=4. The inset presents the dependence of τ/N_A on N_P/N_A. Error bars correspond to standard deviations.

The dependence of τ on f_a, N_A, and N_P at large f_a and k_b can be understood quantitatively using the following dynamical model. When k_b and f_a are large, polymer P translocates through the pore quickly pulled by rod-like polymer A. Assuming that polymer A is a rigid rod and all the monomers in the *trans* side move with a same velocity v, the effective pulling force polymer A exerting on polymer P can be expressed as Eq. (20).

$$F_a \approx N_A f_a \tag{20}$$

and the friction force is

$$f = \eta n v \tag{21}$$

where n is the total number of monomers in the *trans* side.

In the overdamped limit, the pulling force is balanced by the friction force, *i.e.*, $F_a = f$, so

$$v = \frac{N_A f_a}{n\eta} \tag{22}$$

Since $v \propto \frac{dn}{dt}$, we have,

$$\frac{dn}{dt} \sim \frac{N_A f_a}{\eta n} \tag{23}$$

and

$$\int_0^\tau dt \sim \int_{N_A}^{N_P+N_A} \frac{\eta n}{N_A f_a} dn \tag{24}$$

We can calculate the translocation time τ from Eq. (24),

$$\tau \sim \frac{\eta}{f_a N_A}\left[(N_A + N_P)^2 - N_A^2\right] \tag{25}$$

or

$$\frac{\tau}{N_A} \sim \frac{\eta}{f_a}\left[\left(1 + \frac{N_P}{N_A}\right)^2 - 1\right] \tag{26}$$

This is in good agreement with the simulation results shown in the inset of Fig. 9.

Specially, when $N_P >> N_A$, we can get from Eq. (25) that

$$\tau \propto \frac{N_P^2}{f_a N_A} \tag{27}$$

This is in good agreement with the result of passive poly-

mer translocation through a small pore, driven by a strong ending pulling force.[30,31]

Translocation Details

We have found above that there are three translocation mechanisms, coil-diffusion, spiral-winch, and rod-pulling, depending on f_a and k_b. To better distinguish these three mechanisms, we further studied the details of the translocation process. Here, we chose three sets of parameters: Case I (f_a=0.4, k_b=0, N_A=20, N_P=100), Case II (f_a=4, k_b=0, N_A=20, N_P=100), and Case III (f_a=4, k_b=50, N_A=20, N_P=100), under which the polymer translocation is governed respectively by the three mechanisms mentioned above.

Fig. 10 shows the evolution of the translocation coordinate m (or the number of passive monomers entering the *trans* side). We can see that the result of Case I is very different from those of Cases II and III. For Case I, m increases slowly and concavely with time t, and the instantaneous monomer flux, dm/dt, is very small and decreases monotonically, indicating that polymer P moves more and more slowly in the coil-diffusion translocation mechanism. For Cases II and III, the variation of m with t shows similar behavior. At small t, m increases rapidly and concavely, while at larger t, m increases almost linearly. Correspondingly, with t increasing, dm/dt decreases gradually and tends to reach a steady value at large t.

We have also calculated the waiting time t_w for all monomers in polymer P. t_w of monomer s is defined as the average time between the events that monomer s and monomer s+1 enter the *trans* side. Fig. 11 presents the distribution of the waiting time t_w for the three cases of parameter sets. In all three cases, the waiting time varies non-monotonically with s. For Case III, the waiting time first increases and then decreases with s, and exhibits a peak near the end of polymer P, which is consistent with the results of the end-pulling translocation.[30] While for Case I, the peak is near the middle of polymer P, which is similar to the results of pore-driven translocation,[31] indicating that the effective pulling force of polymer A with small f_a on polymer P is negligible. Interestingly, for Case II, the waiting time as a function of s shows two peaks, one near the polymer head and the other near the polymer end, which is related to the formation of the spiral structure of polymer A. Under the parameter conditions of Case II, the active polymer chain rapidly forms a spiral structure at the early stage of polymer P translocation. Before forming the spiral structure, polymer A adopts a quasi-coil conformation (as shown in Fig. 5), exerting a relatively small pulling force on polymer P, so t_w increases rapidly with s. Once the spiral is formed, the effective pulling force exerted by polymer A on polymer P becomes larger, resulting in a rapid decrease in t_w and thus the emergence of the first peak near the head of polymer P. During the subsequent process, the spiral grows, and then the rotational resistance increases gradually, leading to the continuous increase of t_w and the emergence of the second peak near the polymer end.

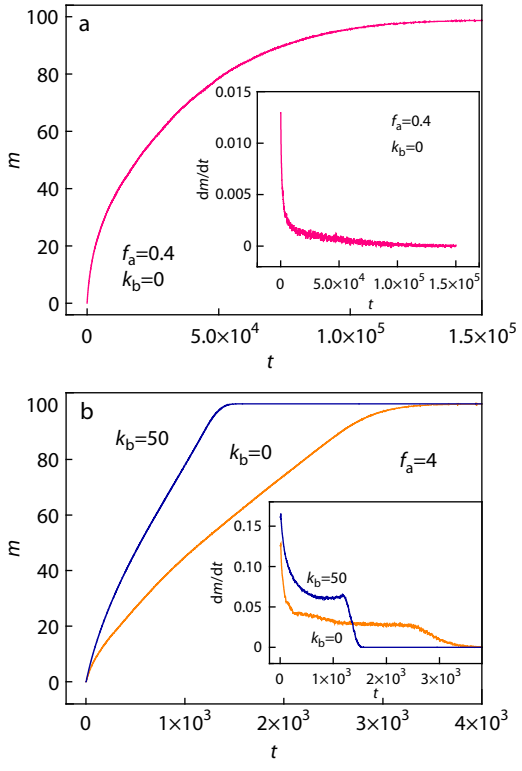

Fig. 10 Evolution of the translocation coordinate m for (a) Case I (f_a=0.4, k_b=0, N_A=20, N_P=100), (b) Case II (f_a=4, k_b=0, N_A=20, N_P=100), and Case III (f_a=4, k_b=50, N_A=20, N_P=100). The insets show the evolution of the instantaneous monomer flux dm/dt.

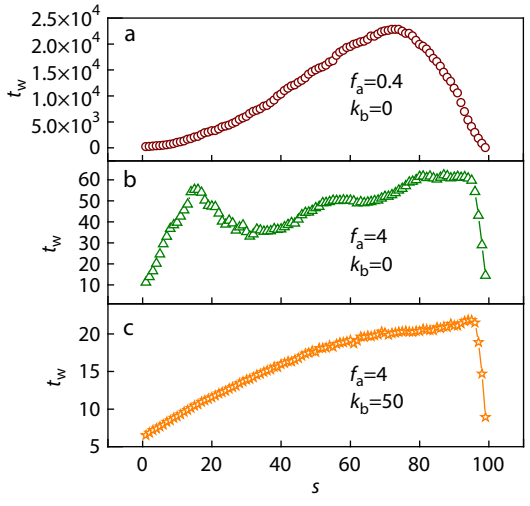

Fig. 11 Distribution of the waiting time t_w for (a) Case I (f_a=0.4, k_b=0, N_A=20, N_P=100), (b) Case II (f_a=4, k_b=0, N_A=20, N_P=100), and (c) Case III (f_a=4, k_b=50, N_A=20, N_P=100).

CONCLUSIONS

The translocation of a passive polymer chain (polymer P) through a small pore pulled by an active polymer chain (polymer A) was studied using Langevin dynamics simulations. Both polymer P and polymer A are modelled by bead-spring chains, and each bead of polymer A is subjected to a tangential self-propelled force (f_a) along the backbone of polymer A. Results indicate that the configuration state of polymer A during the translocation process, which is dependent on f_a and its rigidity k_b, has a significant influence on the translocation time of polymer P.

https://doi.org/10.1007/s10118-026-3802-7

For the case k_b is very small (including k_b=0), polymer A shows different conformation states and motion types depending on f_a. When f_a is small, polymer A is nearly random coil and undergoes nearly random diffusion during the translocation process. The translocation of polymer P can be approximately seen as a random diffusion process, leading to a large translocation time. While when f_a is large, polymer A forms a stable spiral and rotates around its mass center. The translocation dynamics of polymer P is determined by a winch-driven mechanism, in which the spiral of polymer A rotates synchronously with a large force torque and pulls polymer P through the pore quickly, resulting that τ is small. For the case k_b is large, polymer A adopts a rod configuration, and the translocation of polymer P is controlled by the translation of the polymer A rod. Moreover, when the length of polymer P, N_P, is large, the dependence of τ on N_P can be described by a power law, $\tau \propto N_P^{\alpha}$, with α~3.1 for small k_b and f_a, α~2.43 for small k_b and large f_a, and α~2 for large k_b and large f_a.

In our work, one of the most important findings is the winch-driven mechanism for polymer translocation, where a self-organizing, rotating active spiral can act as an efficient winch to pull and wind a passive chain. This mechanism is qualitatively different from both the end-pulling and the pore-driven translocations, as reflected in the distinct scaling exponents and the unique composite structure. Our findings may inspire the design of artificial active-polymer-based transport systems and provide new insights into motor-driven biological translocation processes.

We would note that the 2D simulation is chosen to capture the essential rotational dynamics of the active spiral and to facilitate direct visualization. The simulation results we obtained can be well understood by theoretical models, and the winch-driven mechanism is expected to persist in three dimensions, although the detailed morphology may change from a planar spiral to a compact globule.

Moreover, our Langevin dynamics simulation neglects hydrodynamic interactions and is thus suitable for describing dry systems, such as biomacromolecules translocation in the crowded and highly viscous cellular cytoplasm, where the motion is overdamped. Future extensions, including hydrodynamic effects, would be valuable for systems in which the solvent flow plays a significant role.

Conflict of Interests

The authors declare no interest conflict.

Data Availability Statement

The data that support the findings of this study are available from the corresponding author upon reasonable request.

ACKNOWLEDGMENTS

This work was financially supported by the Zhejiang Provincial Natural Science Foundation of China (No. LY20A040004), and the National Natural Science Foundation of China (Nos. 11604232 and 22203060).

REFERENCES

1 Simon, S. M.; Blobel, G. A protein-conducting channel in the endoplasmic reticulum. *Cell* **1991**, *65*, 371–380.
2 Simon, S. M.; Peskin, C. S.; Oster, G. F. What drives the translocation of proteins. *Proc. Natl. Acad. Sci. U. S. A.* **1992**, *89*, 3770–3774.
3 Kindt, J.; Tzlil, S.; Ben-Shaul, A.; Gelbart, W. M. DNA packaging and ejection forces in bacteriophage. *Proc. Natl. Acad. Sci. U. S. A.* **2001**, *98*, 13671–13674.
4 Tzlil, S.; Kindt, J. T.; Gelbart, W. M.; Ben-Shaul, A. Forces and pressures in DNA packaging and release from viral capsids. *Biophys. J.* **2003**, *84*, 1616–1627.
5 Purohit, P. K.; Inamdar, M. M.; Grayson, P. D.; Squires, T. M.; Kondev, J.; Phillips, R. Forces during bacteriophage DNA packaging and ejection. *Biophys. J.* **2005**, *88*, 851–866.
6 Gabashvili, I. S.; Gregory, S. T.; Valle, M.; Grassucci, R.; Worbs, M.; Wahl, M. C.; Dahlberg, A. E.; Frank, J. The polypeptide tunnel system in the ribosome and its gating in erythromycin resistance mutants of L4 and L22. *Mol. Cell* **2001**, *8*, 181–188.
7 Helenius, J.; Ng, D. T. W.; Marolda, C. L.; Walter, P.; Valvano, M. A.; Aebi, M. Translocation of lipid-linked oligosaccharides across the ER membrane requires Rft1 protein. *Nature* **2002**, *415*, 447–450.
8 Marenduzzo, D.; Micheletti, C.; Orlandini, E.; Sumners, D. W. Topological friction strongly affects viral DNA ejection. *Proc. Natl. Acad. Sci. U. S. A.* **2013**, *110*, 20081–20086.
9 Lam, E. T.; Hastie, A.; Lin, C.; Ehrlich, D.; Das, S. K.; Austin, M. D.; Deshpande, P.; Cao, H.; Nagarajan, N.; Xiao, M.; Kwok, P. Y. Genome mapping on nanochannel arrays for structural variation analysis and sequence assembly. *Nat. Biotechnol.* **2012**, *30*, 771–776.
10 Marie, R.; Pedersen, J. N.; Bauer, D. L. V.; Rasmussen, K. H.; Yusuf, M.; Volpi, E.; Flyvbjerg, H.; Kristensen, A.; Mir, K. U. Integrated view of genome structure and sequence of a single DNA molecule in a nanofluidic device. *Proc. Natl. Acad. Sci. U. S. A.* **2013**, *110*, 4893–4898.
11 Reisner, W.; Larsen, N. B.; Silahtaroglu, A.; Kristensen, A.; Tommerup, N.; Tegenfeldt, J. O.; Flyvbjerg, H. Single-molecule denaturation mapping of DNA in nanofluidic channels. *Proc. Natl. Acad. Sci. U. S. A.* **2010**, *107*, 13294–13299.
12 Polonsky, S.; Rossnagel, S.; Stolovitzky, G. Nanopore in metal-dielectric sandwich for DNA position control. *Appl. Phys. Lett.* **2007**, *91*, 153103.
13 Luan, B.; Stolovitzky, G.; Martyna, G. Slowing and controlling the translocation of DNA in a solid-state nanopore. *Nanoscale* **2012**, *4*, 1068–1077.
14 Glasgow, J.; Tullman-Ercek, D. Production and applications of engineered viral capsids. *Appl. Microbiol. Biotechnol.* **2014**, *98*, 5847–5858.
15 Dorfman, K. D. DNA electrophoresis in microfabricated devices. *Rev. Mod. Phys.* **2010**, *82*, 2903–2947.
16 Han, J.; Craighead, H. G. Separation of long DNA molecules in a microfabricated entropic trap array. *Science* **2000**, *288*, 1026–1029.
17 Kasianowicz, J. J.; Brandin, E.; Branton, D.; Deamer, D. W. Characterization of individual polynucleotide molecules using a membrane channel. *Proc. Natl. Acad. Sci. U. S. A.* **1996**, *93*, 13770–13773.
18 Magill, M.; Falconer, C.; Waller, E.; de Haan, H. W. Translocation time through a nanopore with an internal cavity is minimal for polymers of intermediate length. *Phys. Rev. Lett.* **2016**, *117*, 247802.
19 Chen, K.; Jou, I.; Ermann, N.; Muthukumar, M.; Keyser, U. F.; Bell, N.

Graphical Abstract

Translocation of a Long Passive Polymer Chain through a Small Pore Pulled by an Active Polymer Chain

Yan-Li Zhou, Xiao Yang, Bin Zhao, and Chao Wang

Taizhou University

The active polymer with low rigidity and high activity forms a spiral in the *trans* side, and acts as a rotating winch pulling the passive polymer through the pore and winding it sequentially around itself.

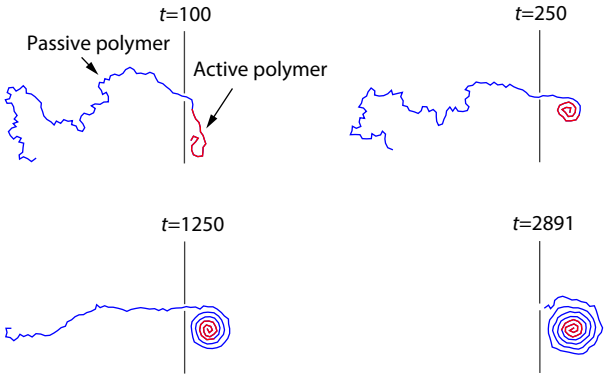

Chinese J. Polym. Sci. 2026 *https://doi.org/ 10.1007/s10118-026-3802-7*

A. W. Dynamics of driven polymer transport through a nanopore. *Nat. Phys.* **2021**, *17*, 1043−1049.
20 Ding, M.; Duan, X.; Lu, Y.; Shi, T. Flow-induced ring polymer translocation through nanopores. *Macromolecules* **2015**, *48*, 6002−6007.
21 Ding, M.; Li, L. Flow-induced translocation and conformational transition of polymer chains through nanochannels: recent advances and future perspectives. *Macromolecules* **2021**, *54*, 9773−9793.
22 Wang, Z.; Wang, R.; Lu, Y.; An, L.; Shi, A. C.; Wang, Z. G. Mechanisms of flow-induced polymer translocation. *Macromolecules* **2022**, *55*, 3602−3612.
23 Li, X.; Pivkin, I. V.; Liang, H. Hydrodynamic effects on flow-induced polymer translocation through a microfluidic channel. *Polymer* **2013**, *54*, 4309−4317.
24 Ambjörnsson, T.; Lomholt, M. A.; Metzler, R. Directed motion emerging from two coupled random processes: translocation of a chain through a membrane nanopore driven by binding proteins. *J. Phys.: Condens. Matter* **2005**, *17*, S3945−S3964.
25 Abdolvahab, R. H.; Ejtehadi, M. R.; Metzler, R. Sequence dependence of the binding energy in chaperone-driven polymer translocation through a nanopore. *Phys. Rev. E* **2011**, *83*, 011902.
26 Yu, W.; Luo, K. Chaperone-assisted translocation of a polymer through a nanopore. *J. Am. Chem. Soc.* **2011**, *133*, 13565−13570.
27 Turner, S. W. P.; Cabodi, M.; Craighead, H. G. Confinement-induced entropic recoil of single DNA molecules in a nanofluidic structure. *Phys. Rev. Lett.* **2002**, *88*, 128103.
28 Wang, C.; Wu, F.; Zhao, B.; Chen, Y. C.; Luo, M. B. Spontaneous injection of polymer into a spherical cavity from a narrow tube. *Macromolecules* **2020**, *53*, 1694−1700.
29 Huang, H. C.; Hsiao, P. Y. Scaling behaviors of a polymer ejected from a cavity through a small pore. *Phys. Rev. Lett.* **2019**, *123*, 267801.
30 Huopaniemi, I.; Luo, K.; Ala-Nissila, T.; Ying, S. C. Polymer translocation through a nanopore under a pulling force. *Phys. Rev. E* **2007**, *75*, 061912.
31 Sarabadani, J.; Ala-Nissila, T. Theory of pore-driven and end-pulled polymer translocation dynamics through a nanopore: an overview. *J. Phys.: Condens. Matter* **2018**, *30*, 274002.
32 Menais, T. Polymer translocation under a pulling force: scaling arguments and threshold forces. *Phys. Rev. E* **2018**, *97*, 022501.
33 Huopaniemi, I.; Luo, K.; Ala-Nissila, T.; Ying, S. C. Langevin dynamics simulations of polymer translocation through nanopores. *J. Chem. Phys.* **2006**, *125*, 124901.
34 Sáinz-Agost, A.; Falo, F.; Fiasconaro, A. Polymer translocation driven by longitudinal and transversal time-dependent end-pulling forces. *Phys. Rev. E* **2023**, *108*, 034501.
35 Adane, M.; Tatek, Y. B.; Tilahun, M. Transport of a comb-like polymer across a nanochannel subject to a pulling force. *J. Phys.: Condens. Matter* **2024**, *36*, 505103.
36 Tilahun, M.; Tatek, Y. B. End-pulled translocation of a star polymer out of a confining cylindrical cavity. *Macromol. Theory Simul.* **2021**, *30*, 2000090.
37 Chen, X.; Chen, J.; Zhuo, B. Y.; Yang, X.; Luo, M. B. Simulation study for the pulling translocation of a polymer globule. *Polym. J.* **2021**, *53*, 1047−1056.
38 Fiasconaro, A.; Díez-Señorans, G.; Falo, F. End-pulled polymer translocation through a many-body flexible pore. *Polymer* **2022**, *259*, 125305.
39 Hu, H. X.; Shen, Y. F.; Luo, M. B. Translocation of two-dimensional active polymers through nanopores using Langevin dynamics simulations. *J. Chem. Phys.* **2024**, *160*, 184902.
40 Chuang, J.; Kantor, Y.; Kardar, M. Anomalous dynamics of translocation. *Phys. Rev. E* **2001**, *65*, 011802.
41 Kantor, Y.; Kardar, M. Anomalous dynamics of forced translocation. *Phys. Rev. E* **2004**, *69*, 021806.
42 Luo, K.; Ollila, S. T. T.; Huopaniemi, I.; Ala-Nissila, T.; Pomorski, P.; Karttunen, M.; Ying, S. C.; Bhattacharya, A. Dynamical scaling exponents for polymer translocation through a nanopore. *Phys. Rev. E* **2008**, *78*, 050901(R).
43 Luo, M. B.; Cao, W. P. Influence of polymer-pore interaction on the translocation of a polymer through a nanopore. *Phys. Rev. E* **2012**, *86*, 031914.
44 Luo, K.; Huopaniemi, I.; Ala-Nissila, T.; Ying, S. C. Polymer translocation through a nanopore under an applied external field. *J. Chem. Phys.* **2006**, *124*, 114704.
45 Luo, K.; Metzler, R. Polymer translocation into a fluidic channel through a nanopore. *Phys. Rev. E* **2010**, *82*, 021922.
46 Zhang, Y.; Tian, W. D. Recent progress in non-equilibrium structure and dynamics of connected active agents. *J. Phys.:*

Condens. Matter **2025**, *37*, 143002.
47 Isele-Holder, R. E.; Elgeti, J.; Gompper, G. Self-propelled worm-like filaments: spontaneous spiral formation, structure, and dynamics. *Soft Matter* **2015**, *11*, 7181–7190.
48 Man, Y.; Kanso, E. Morphological transitions of axially-driven microfilaments. *Soft Matter* **2019**, *15*, 5163–5173.
49 Wu, J. C.; Lin, F. J.; Ai, B. Q. Absolute negative mobility of active polymer chains in steady laminar flows. *Soft Matter* **2022**, *18*, 1194–1200.
50 Khalilian, H.; Peruani, F.; Sarabadani, J. Structural dynamics and optimal transport of an active polymer. *Soft Matter* **2024**, *20*, 7592–7600.
51 Bianco, V.; Locatelli, E.; Malgaretti, P. Globulelike conformation and enhanced diffusion of active polymers. *Phys. Rev. Lett.* **2018**, *121*, 217802.
52 Locatelli, E.; Bianco, V.; Malgaretti, P. Activity-induced collapse and arrest of active polymer rings. *Phys. Rev. Lett.* **2021**, *126*, 097801.
53 Chelakkot, R.; Gopinath, A.; Mahadevan, L.; Hagan, M. F. Flagellar dynamics of a connected chain of active, polar, Brownian particles. *J. R. Soc. Interface* **2014**, *11*, 20130884.
54 Fily, Y.; Subramanian, P.; Schneider, T. M.; Chelakkot, R.; Gopinath, A. Buckling instabilities and spatio-temporal dynamics of active elastic filaments. *J. R. Soc. Interface* **2020**, *17*, 20190794.
55 Ng'ang'a, D. K.; Kang'iri, S. M.; Hess, H.; Nitta, T. Active spiralling of microtubules driven by kinesin motors. *Sci. Rep.* **2025**, *15*, 20318.
56 Wang, C.; Zhou, Y.; Yang, X.; Chen, Y.; Shen, Y.; Luo, M. Conformation and dynamics of a tethered active polymer chain. *Phys. Rev. E* **2022**, *106*, 054501.
57 Li, J. X.; Wu, S.; Hao, L. L.; Lei, Q. L.; Ma, Y. Q. Activity-driven polymer knotting for macromolecular topology engineering. *Sci. Adv.* **2024**, *10*, eadr0716.
58 Wu, S.; Li, J. X.; Ma, Y. Q. Conformation and dynamics of active polymers with one end fixed. *Phys. Rev. E* **2025**, *112*, 045431.
59 Shen, C.; Qin, C. R.; Xu, T. L.; Chen, K.; Tian, W. D. Structure and dynamics of an active polymer adsorbed on the surface of a cylinder. *Soft Matter* **2022**, *18*, 1489–1497.
60 Wang, Y.; Gao, Y. W.; Tian, W. D.; Chen, K. Obstacle-induced giant jammed aggregation of active semiflexible filaments. *Phys. Chem. Chem. Phys.* **2022**, *24*, 23779–23789.
61 Wu, S.; Li, J. X.; Lei, Q. L. Facilitated dynamics of an active polymer in 2D crowded environments with obstacles. *Soft Matter* **2022**, *18*, 9263–9272.
62 Mokhtari, Z.; Zippelius, A. Dynamics of active filaments in porous media. *Phys. Rev. Lett.* **2019**, *123*, 028001.
63 Heeremans, T.; Deblais, A.; Bonn, D.; Woutersen, S. Chromatographic separation of active polymer-like worm mixtures by contour length and activity. *Sci. Adv.* **2022**, *8*, eabj7918.
64 Yang, X.; Zhou, Y. L.; Zhao, B.; Wang, C.; Luo, M. B. Conformation and dynamics of a long active polymer chain confined in a circular cavity. *Chinese J. Polym. Sci.* **2025**, *43*, 225–234.
65 Wang, C.; Hu, H. X.; Zhou, Y. L.; Zhao, B.; Luo, M. B. Translocation of a self-propelled polymer through a narrow pore. *Chinese J. Polym. Sci.* **2022**, *40*, 1670–1678.
66 Tan, F.; Yan, R.; Zhao, C.; Zhao, N. Translocation dynamics of an active filament through a long-length scale channel. *J. Phys. Chem. B* **2023**, *127*, 8603–8615.
67 Xu, G. H.; Li, F. G.; Wu, J. C.; Ai, B. Q. Rectification of an active polymer chain with chirality in a transversal asymmetric channel. *Phys. A Stat. Mech. Appl.* **2021**, *575*, 126051.
68 Wang, C.; Zhou, Y. L.; Yang, X.; Wu, F.; Luo, M. B. Injection of a self-propelled polymer into a small circular cavity. *Chinese J. Polym. Sci.* **2024**, *42*, 886–894.
69 Rezaie-Dereshgi, A.; Khalilian, H.; Sarabadani, J. Translocation of an active polymer into a two dimensional circular nano-container. *J. Phys.: Condens. Matter* **2023**, *35*, 355101.
70 Isele-Holder, R. E.; Jäger, J.; Saggiorato, G.; Elgeti, J.; Gompper, G. Dynamics of self-propelled filaments pushing a load. *Soft Matter* **2016**, *12*, 8495–8505.
71 Manna, R. K.; Kumar, P. B. S.; Adhikari, R. Colloidal transport by active filaments. *J. Chem. Phys.* **2017**, *146*, 024901.
72 Sung, W.; Park, P. J. Polymer translocation through a pore in a membrane. *Phys. Rev. Lett.* **1996**, *77*, 783–786.

https://doi.org/10.1007/s10118-026-3802-7